

Free energy conservation in *ab initio* molecular dynamics simulations and homogeneous melt nucleation

Ming Geng (耿明)^{1,2} and Chris E. Mohn^{1,2,3*}

¹Centre for Planetary Habitability (PHAB), University of Oslo, N-0315 Oslo, Norway

²Centre for Earth Evolution and Dynamics (CEED), University of Oslo, N-0315 Oslo, Norway and

³Department of Chemistry and Center for Materials Science and Nanotechnology, University of Oslo, Oslo 0371, Norway

(Dated: August 9, 2023)

The Z method is a popular atomistic simulation method for determining the melting temperature of solids by using a sequence of molecular dynamics (MD) runs in the microcanonical (NVE) ensemble to target the lowest system energy where the solid always melts. Homogeneous melting at the superheating critical limit (T_h), is accompanied by a temperature drop to the equilibrium melting temperature (T_m). Implementation of the Z method interfaced with modern *ab initio* electronic structure packages use Hellman-Feynman dynamics to propagate the ions in the NVE ensemble with the Mermin free energy plus the ionic kinetic energy conserved. So the electronic temperature (T_{el}) is kept fixed along the trajectory which may introduce some spurious ion-electron interactions in MD runs with large temperature changes. We estimate possible systematic errors in evaluating melting temperature with different choices of T_{el} . MD runs with the $T_{el} = T_h$ and $T_{el} = T_m$ shows that the difference in melting temperature can be 200-300 K (3-5% of the melting temperature) for our two test systems. Our results are in good agreement with previous studies with different methods, suggesting the CaSiO_3 and SiO_2 melts at around 6500 at 100 GPa and 6000 K at 160 GPa. The melting temperature decreases with increasing T_{el} due to the increasing entropic stabilisation of the liquid and the system melts about 3 times faster with $T_{el} = T_h$ than with $T_{el} = T_m$. A careful choice of T_{el} in BOMD is essential for the critical evaluation of the Z method especially at very high temperatures. Inspection of the homogeneous melting process shows that melting occurs via a two-step mechanism: 1) melting of the anion sublattice is accompanied by a small drop in temperature and 2) the formation of small defects which trigger the formation of small liquid clusters and fully melted.

I. INTRODUCTION

Melting and solidification processes are ubiquitous in condensed matter physics and in the evolution of terrestrial bodies including our own Earth. Triggered by extended defects, grain boundaries or open surfaces, equilibrium melting occurs spontaneously at T_m when the free energy of the solid equals that of the liquid. Under certain conditions, however, a crystal can melt *homogeneously* at a much higher temperature, T_h , which represents the critical limit of superheating before melting is unavoidable [1, 2]. If a perfect periodic crystal in a molecular dynamics simulation is heated until $T \approx T_h$, spontaneous fluctuations (nucleation precursors) will form transient defects and liquid nuclei which trigger an irreversible rapid nucleation growth and melting. Although homogeneous melting is rare in nature, shock-induced homogeneous melting has been demonstrated in a number of experiments (see for example [3–6]).

Atomistic simulation explores the link between homogeneous and equilibrium melting using molecular dynamics simulations and has been widely used to estimate melting temperatures for different materials [7–10] often at high temperatures and pressure where experiments are hazardous or impractical [11–16]. With the Z method, a number of molecular dynamics simulations are launched

in the microcanonical (NVE) ensemble at different initial temperatures, T_{ini} , to target the lowest total energy, E_h , where the solid always melts. When the system melts at $E_h(T_h)$, the temperature decreases to the equilibrium melting temperature while the latent heat of melting gradually converts into potential energy. If we assume a linear variation of energy with temperature we can establish a relationship between T_h and T_m from the entropy of melting [1, 17]:

$$\frac{T_h}{T_m} - 1 = \frac{\Delta S_m}{C_V} \quad (1)$$

where C_V is the heat capacity at constant volume of the solid and ΔS_m is the entropy of melting. Eq. 1 can be approximated by $\ln 2/3$ assuming an ideal entropy of melting ($3k_B$ (per atom)) taken from a high-temperature limit of the Debye model and assuming that the heat capacity at constant volume is given by $k_B \ln 2$ (per atom) when $\Delta V_m/V \rightarrow 0$ [18].

Since the equilibrium melting temperature can be calculated from a homogeneous melting at T_h triggered typically by small defects, quite small simulation boxes (~ 100 atoms) are in general sufficient to accurately calculate T_h and hence T_m from Eq. 1 [19]. The use of small simulation boxes therefore makes the Z method an attractive potentially computational "low-cost" method for the accurate calculation of melting temperature [19–21]. By contrast, popular two-phase approaches to melting where the equilibrium melting process is mimicked by constructing a simulation box with solid and liquids

* chris.mohn@kjemi.uio.no

in mechanical contact, often require large boxes to accommodate both solid and liquid phases and their interface [22, 23]. In addition, since T_m can be calculated from Eq. 1, there is no need for the explicit calculation of free energies which sometimes hamper the precision of thermodynamic integration [24, 25] and 2PT methods [26], especially when the solid and liquid free energy curves have very similar steepness near T_m [22, 27].

In spite of these advantages, recent studies have unveiled some artificial features that may hamper the Z method for the accurate calculation of melting temperatures in particular under extreme conditions [20, 22]. Since the waiting time required for the solid to melt diverges in the limit where $T_{\text{ini}} \rightarrow T_h$, a waiting time analysis is often carried out at different $T_{\text{ini}} > T_h$ to estimate T_m from extrapolation to that of "infinite" waiting-time [20]. This analysis, however, may still require extensive statistics for the precise calculation of melting temperatures.

Moreover, Born-Oppenheimer *ab initio* molecular dynamics (BOMD) is typically performed in the NVE ensemble using Hellman-Feynman dynamics where the Fermi-Dirac electronic temperature is *kept fixed* in the MD simulation [28]. Although this implementation ensures conserved dynamics [29, 30], large changes in temperature following melting and sometimes equilibration, may introduce systematic errors in T_m since the electronic temperature is kept fixed [22]. For the Z method, two (solid/liquid) phases with large temperature differences exist in the same simulation trajectory at different time ranges, especially for an insulator or semiconductor. A BOMD NVE run with $E > E_h$ is launched with an T_{el} chosen near the melted liquid temperature ($T_{\text{el}} \approx T_m$), then the T_{el} will be much lower than the temperature in the solid state (before melting). A too low electronic entropy may favour the stabilisation of the solid and prevent melting. This will affect the estimated homogeneous melting temperature (T_h) and the "waiting time" for a solid to melt. The calculated equilibrium melting temperature may therefore be too high. On the other hand, if a BOMD run is launched with an electronic temperature chosen near the solid temperature before melting ($T_{\text{el}} \approx T_h$). Therefore, it will give a reasonable electronic-ionic coupling before melting. However, once the solid melts at constant volume the temperature drops by $1 - T_m/T_h \approx \ln 2/3$ and the electronic entropy will be much higher than the liquid temperature, which usually favours an entropic stabilisation of the liquid. Hence, the melting temperature may be too low. Therefore, since the coupling between electronic and ionic degrees of freedom in BOMD NVE runs may be significant following the large temperature drops, addressing the sensitivity in melting temperature to the choice of T_{el} is crucial.

In this work, we thus investigate the role of electronic entropy on homogeneous melting for two main abundant mineral components in the Earth's interior CaSiO_3 and SiO_2 at high temperatures.

Ca-perovskite is the third most abundant mineral in

the lower mantle and a main component of basaltic lithologies constituting more than 20% of recycled oceanic crust that is continuously being injected into the Earth's deep interior. A strong preferential partitioning of radioactive heat-producing elements into CaSiO_3 , such as U and Th, as well as key geochemical tracers suggests that CaSiO_3 is the main storage minerals for many of these minority elements [31, 32]. Tracking the distribution of CaSiO_3 in the lowermost mantle is therefore essential to understand the evolution of the solid Earth which in turn requires the thermodynamic conditions of Ca-perovskite melting. Motivated by this, a number of computational studies have calculated melting-curve for pure CaSiO_3 to lowermost mantle conditions [17, 22], but the agreement is not satisfactory. Here we attempt to contribute to tighten the constraints of CaSiO_3 melting at the lowermost mantle conditions.

Our second model system is SiO_2 . The solid-liquid phase boundary of SiO_2 at ultrahigh pressure is critical to our understanding of not only the Earth's evolution but also the formation of many super-Earths [33, 34]. High-pressure silica melting may also play an important role in core dynamics, as it has been suggested that silica may have crystallized from a Si-saturated proto-core during a chemical exchange with a basal magma ocean [35, 36]. In spite of a number of simulations and experimental results reported in the literature, the SiO_2 melting curve remains poorly constrained at very high pressure. Here we will attempt to contribute to resolving some of these outstanding discrepancies in order to help tighten the constraints on silica melting.

Since *ab initio* MD simulations allow detailed insight into homogeneous melting processes we shall take the opportunity to investigate melting nucleation processes in these systems. Atomistic insight into the formation of defect formation triggering homogeneous melting remains poorly explored and is extremely difficult to capture experimentally.

II. THEORY

The classical thermodynamic ensemble appropriate for the Z method is microcanonical (NVE ensemble) with the volume, V , number of species N and the total system energy, E , kept fixed. The maximum energy along the solid branch of the isochore, E_h , is the same as the lowest energy along the liquid branch:

$$E_{\text{sol}}(V, T_h) = E_{\text{liq}}(V, T_m). \quad (2)$$

To locate $E_{\text{sol}}(V, T_h)$ and/or $E_{\text{liq}}(V, T_m)$, a sequence of NVE MD runs are carried out with different initial temperatures. Since the waiting time for the solid to melt diverges when $T \rightarrow T_h$, the calculated melting temperature will always represent an upper bound to the "true" melting temperature. To avoid extremely long MD runs in the vicinity of T_h , the melting temperature is calculated from an extrapolation of the distributions of waiting

times for a sequence of runs with different energies $> E_h$ using

$$\tau^{-1/2} = A(T_{\text{liq}} - T_m) \quad (3)$$

where "A" is a parameter and τ is the waiting time for a solid to melt at a given total energy and T_{liq} is the liquid temperature of the system after melting. $T_{\text{liq}} = T_m$, when $E = E_h$. The melting temperature is then found at infinite waiting time (i.e. at the point of intersection where $\tau^{-1/2} = 0$).

We use *ab initio* Born-Oppenheimer MD to calculate the system total energy where the electronic energy is minimized at each step along the ionic trajectory. Note that the usual Hellmann-Feynman dynamics do not conserve the total system energy, $E = U + K$ where U is the internal DFT energy and K is the kinetic energy of the ions. This is because the energy functional is non-variational with respect to changes in partial orbital occupancies along the MD trajectory.

To avoid additional contributions to the Hellmann-Feynman forces due to the variation in the band occupancies along the ionic trajectory the quantity " $K + \Omega$ ", rather than the total energy, is conserved in the MD run where Ω is the Mermin free-energy [29, 30, 37]

$$\Omega = U - T_{\text{el}} S_{\text{el}} \quad (4)$$

with

$$S_{\text{el}} = -k_B \sum_i [f_i \ln f_i + (1 - f_i) \ln(1 - f_i)]. \quad (5)$$

S_{el} is the electronic entropy and f_i is the electron occupancy of band i calculated using Fermi-Dirac statistics:

$$f_i = F\left(\frac{\epsilon_i - E_{\text{fermi}}}{\sigma}\right), \sum_0^{N_i} f_i = N \quad (6)$$

where F is the usual (Fermi-Dirac) smearing function, ϵ_i is the eigenvalue of band i , E_{fermi} is the Fermi level and $\sigma = k_B/T$ is the smearing broadening.

In the microcanonical ensemble, however, large temperature changes following equilibrium and melting may significantly affect the coupling between ionic and electronic degrees of freedom for many semiconductors and insulators even though the fractional occupancies following these large temperature changes remain small.

We can estimate the sensitivity in the calculated T_m to choices of T_{el} by comparison of the melting temperature calculated using $T_{\text{el}} \approx T_h$ with that calculated $T_{\text{el}} \approx T_m$. These choices of T_{el} will give reasonable upper and lower bounds to the calculated melting temperature in the microcanonical ensemble when the Hellmann-Feynman forces are used for the ionic propagation with $K + \Omega$ being conserved.

If changes in T_{el} can not be ignored, the usual Mermin functional may not be appropriate in the form of Eq. 4, because dynamics is sensitive to choices of T_{el} .

The forces include contributions arising due to changes in the partial orbital occupancies along the microcanonical Born-Oppenheimer MD trajectory. It is important to note, however, that the time evolution of orbital occupancies due to large temperature changes is only correctly described by the time-dependent Schrödinger equation.

A possible strategy to calculate T_m using the Z method is to adjust T_{el} along the ionic trajectory to match the average (ionic) temperature in the previous N time-steps [22]. Although this "update scheme" does not ensure conserved dynamics, the average ensemble temperature before and after adjustment is in general expected to be small. In this approach, the time-dependent Schrödinger equation is thus approximated by a sequence of BOMD NVE simulations.

III. COMPUTATIONAL DETAILS

All BOMD simulations are performed with the Vienna *ab initio* simulation package (VASP) [38, 39], using the projector augmented wave (PAW) method [40, 41]. The exchange-correlation interaction was described using the generalized gradient approximation (GGA) where the exchange-correlation contribution to the energy is parameterized by Perdew, Burke and Ernzerhof (PBE) [42] for SiO_2 and by the Armiento Mattsson, AMO5 functional for CaSiO_3 [43]. The electronic configurations were: $[\text{He}]2s^2 2p^4$ for O, $[\text{Ne}]3s^2 3p^2$ for Si and $[\text{He}]3s^3 p^6 4s^2$ for Ca. The energy cutoff for the plane wave was 700 eV for SiO_2 and somewhat lower, 500 eV, for CaSiO_3 to compare directly with previous CaSiO_3 DFT studies [17, 22].

In all runs, the atoms were placed at their ideal crystallographic sites i.e. the 1b, 1a and 3d positions for Ca, Si and O atoms of the $Pm3m$ space group (CaSiO_3). SiO_2 was started from the ideal pyrite-type structure ($Pa\bar{3}$) optimized to target an equilibrium pressure ~ 160 GPa. This is probably slightly below the stability field of the pyrite structured SiO_3 near the melting curve [33], but in order to compare directly with results in Ref. [21, 34] we use pyrite rather than seifertite. The estimated melting point when pyrite is used as the crystal structure is only slightly lower compared to that found using seifertite. [21, 34]. For CaSiO_3 we used a cubic 135 atoms simulation box which is the same as that used in previous computational studies of CaSiO_3 melting [17, 22] allowing for a direct comparison with these studies. For SiO_2 pyrite the box was cubic and contained 96 atoms.

Melting simulations are carried out in the NVE ensemble with a timestep of 0.5 fs for SiO_2 and 1 ps for CaSiO_3 . The smaller timestep for SiO_2 was chosen to minimize the energy fluctuation. All runs used in the calculation of the waiting time were carried out until melting plus an additional 5-20 ps to calculate the average liquid temperature.

Waiting time analysis were performed based on at least 10 different simulations at a given total energy, volume and initial atom positions where, in each run, the

forces were taken from a Maxwell-Boltzmann distribution. Close to the homogeneous melting temperature we performed typically around 20 MD runs at a given (E, V) to ensure that sufficient statistics was collected in order to calculate τ using Eq. 3. All MD calculations launched below E_h , lasted for at least 10 ps and close to T_h the MD simulations typically ran for more than 100 ps.

For SiO_2 the T_{el} are 6000, 7000 and 8000 K where 6000 K is expected, after test-calculations, to lie close to T_m whereas 8000 K will lie close to T_h . Similarly, for CaSiO_3 the waiting time analysis was carried out at $T_{el} = 6500$ K and 9000 K which are expected to be close to T_m and T_h respectively. To simulate melting with negligible contribution from the electronic entropy we used a Gaussian scheme [28] with a very low value of the smearing parameter (i.e. $\sigma_{\text{Gaussian}} = 0.03$ eV). The Gaussian smearing method is better designed to avoid instabilities arising from fluctuations in orbital occupancies at low values of σ (low temperatures) which often hamper the Fermi-Dirac method during energy minimizations. The Gaussian smearing has the functional form $\frac{1}{2}(1 - \text{erf} \frac{\epsilon - \mu}{\sigma})$ and the link between the two schemes is given by the ratios of the full width at half maximum, FWHM, as:

$$\frac{\text{FWHM}_{\text{FermiDirac}}}{\text{FWHM}_{\text{Gaussian}}} = \frac{\cosh^{-1}(\sqrt{2})}{\sqrt{\ln 2}}. \quad (7)$$

IV. RESULTS AND DISCUSSION

A. Influence of electronic entropy on ionic dynamics

In Fig. 1 we illustrate the sensitivity to changes in electronic temperature on the melting dynamics for silica where the initial ionic temperatures are *the same* in all runs. In the extreme case where the electronic temperature is the same as the initial temperature in the MD runs ($T_{el} = T_{ini} = 18000$ K), SiO_2 always melts rapidly and instantaneously in less than 0.5 ps. On the contrary, in runs with negligible contribution from electronic entropy (i.e. with $\sigma_{\text{Gaussian}} = 0.03$ eV), it is very rare to observe any melting happen, we only observed one incidence of melt-nucleation in all our 20 runs which last 10 ps each.

In simulations with "intermediate" T_{el} , close to either the homogeneous (T_h) or the equilibrium melting temperatures (T_m) (i.e. with $T_{el} = 8000$ K or $T_{el} = 6000$ K) respectively, the system melted markedly slower compared to those with $T_{el} = 18000$ K and the waiting time was much longer. On average, we found that the waiting time median was about 3 ps when $T_{el} = 8000$ K $\approx T_h$ and runs with $T_{el} = 6000 \approx T_m$ are obvious longer (See the discussion about distribution of waiting time in the SI). Interestingly, when $T_{el} = 6000$ K, we observe that the temperature sometimes drops markedly indicating possibly the formation of melt nuclei, but the system quickly reverted to its original (solid) state. This is seen as a

small "bump" in the temperature/pressure evolution in Fig. 1 at about 2.0-2.5 ps. Solid-liquid "oscillations" is often seen in runs where the energy is close to the target homogeneous melting energy using small simulation boxes with large temperature fluctuations [20] and will be discussed more below.

The influence of electronic entropy on properties is also seen in Fig. 2 where two isochores with different electronic temperatures are drawn. Here, the initial ionic temperature in the MD runs is systematically increased from 8000 K to 30000 K. The isochore with an high electronic temperature i.e. close to T_h (i.e. with $T_{el} = 8000$ K) deviates strongly from the one with negligible contributions from electronic entropy (i.e. $\sigma_{\text{Gaussian}} = 0.03$ eV).

B. Choice of electronic temperature in *ab initio* MD runs

The sensitivity in melting temperature to choice of T_{el} illustrated above for SiO_2 and discussed in SI suggests that Born-Oppenheimer MD runs in the NVE ensemble with $\Omega + K$ being conserved may introduce some errors due to changes in electron-ion coupling following large drops in temperature $\approx \ln 2/3 \times T_h$. Indeed, as seen in the Z plots and the waiting-time analysis in Fig. 3 and 4, as well as Table I, for both SiO_2 and CaSiO_3 , when T_{el} is kept fixed at some value near T_m , the calculated equilibrium melting temperature will be markedly higher compared to that if T_{el} is close to the homogeneous melting temperature. The calculated melting temperatures with $T_{el} \approx T_m$ at around 100 GPa (CaSiO_3) and 150 GPa (SiO_2) are about 300 K and 200 K higher respectively than those calculated with $T_{el} \approx T_h$. This corresponds roughly to 10% of the temperature drop accompanying melting. We expect that these absolute errors increase with increasing melting temperature and pressure since the temperature drop accompanying melting increases with increasing T_h .

A key question is therefore: what is the best choice of electronic temperature to minimize the errors in the calculated T_h and T_m ? If we choose an electronic temperature very close to T_h in MD runs with $E = E_h$, the electronic temperature is very close to the (ensemble) average temperature before the system eventually melts. Runs with $T_{el} \approx T_h$ therefore enables the accurate calculation of T_h as well as waiting time and implies that MD runs where $T_{el} < T_h$ (if, say $T_{el} = T_m$) give too high homogeneous melting temperatures.

Although $T_{el} \approx T_h$ (with $E \approx E_h$) enables the accurate calculation of T_h , the melting temperature may be severely underestimated. This is because T_{el} is much larger than the liquid (ionic) temperature which, in general, favours an entropic stabilization of the liquid over the solid and hence the calculated melting temperature will be too low. If we rather chose $T_{el} \approx T_m$, which is the lowest temperature on the isochore, representing a

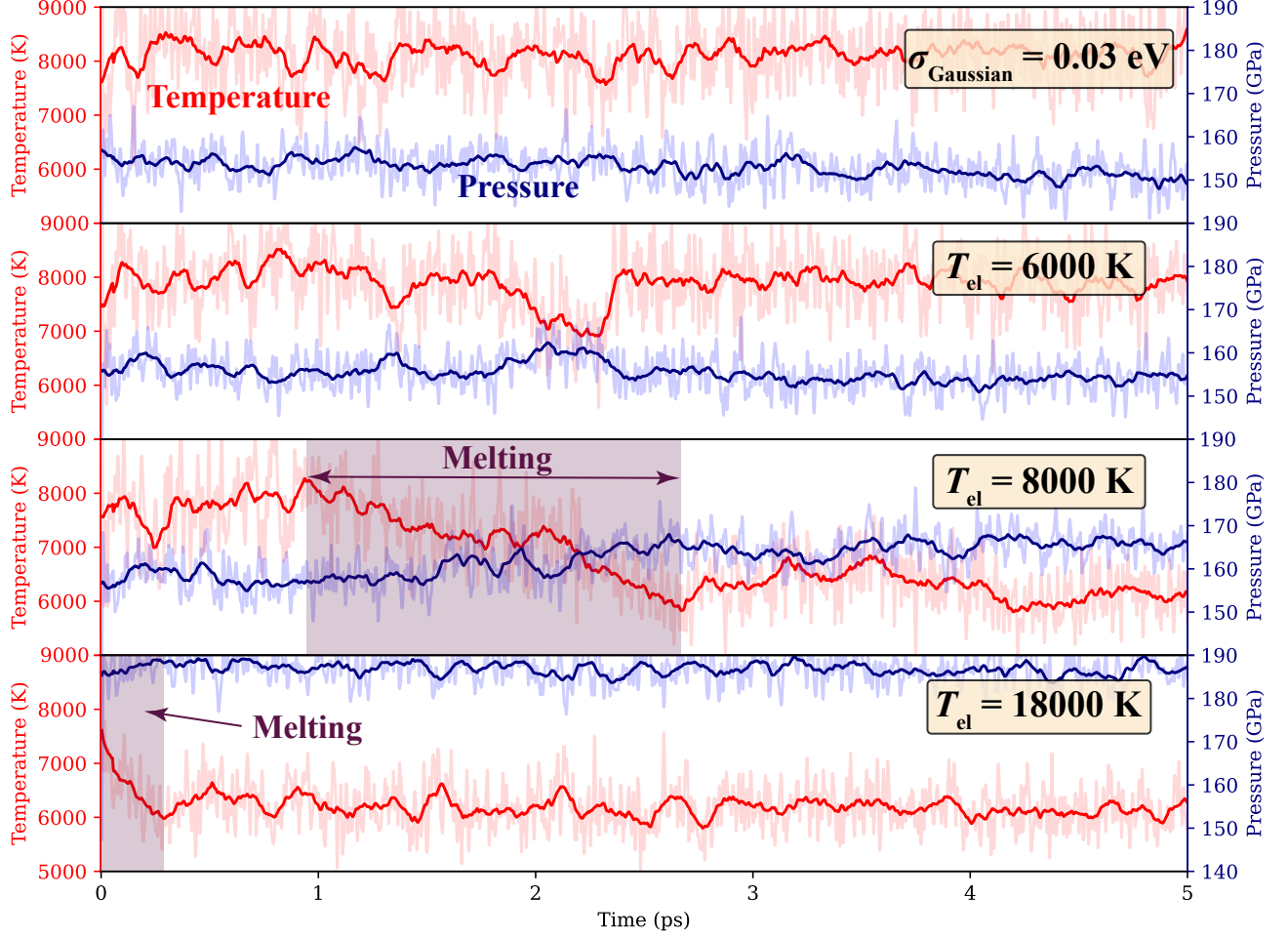


FIG. 1. Temperature (red) and pressure (blue) evolutions along snapshots of *ab initio* MD trajectories with different eT_{el} . The thin lines show dumps every time-step whereas the thick lines are averaged properties over the last 100 time-steps. All MD runs are carried out with the same initial temperature ($T_{ini} = 18000$ K) where the atoms are distributed at their equilibrium lattice positions before we launch the MD run. A Gaussian smearing broadening scheme with $\sigma = 0.03$ eV is used to represent simulations with a negligible contribution to electronic entropy on the ion dynamics. The shaded area shows the melting process.

lower bound to a reasonable choice of T_{el} , the homogeneous melting temperature and possibly the equilibrium melting temperature will be *overestimated*. Calculations where T_{el} is chosen to target either T_m or T_h , therefore, provide reasonable *upper and lower bounds* respectively to the true melting temperature.

C. CaSiO_3 melting

As shown in Table I, our melting temperatures are in very good agreement with a previous Z method study [22] and also in excellent agreement with those from thermodynamic integration and two-phase calculations [22]. The inclusion of electronic entropy is essential for the accurate calculation of melting temperature for CaSiO_3 , in

agreement with that found for other wide band gap insulators such as MgO [44]. That is, the calculated T_h and T_m without contribution from the electronic entropy are about 1000 K and 650 K higher respectively than that calculated using $T_{el} = 6500$ K. We find that the melting temperature is around 6300 K (with $T_{el} = 9000$ K) and 6600 K (with $T_{el} = 6500$ K). As discussed above, the discrepancy between the calculated melting temperature with $T_{el} = 6500$ K and $T_{el} = 9000$ K is non-negligible for the accurate calculation of melting temperature placing some constraints on the accuracy of the Z method implemented with Born-Oppenheimer dynamics in the NVE ensemble.

Choice of electronic entropy could therefore possibly explain the large discrepancy of more than 1000 K between our melting point and a recent Z method result [17]

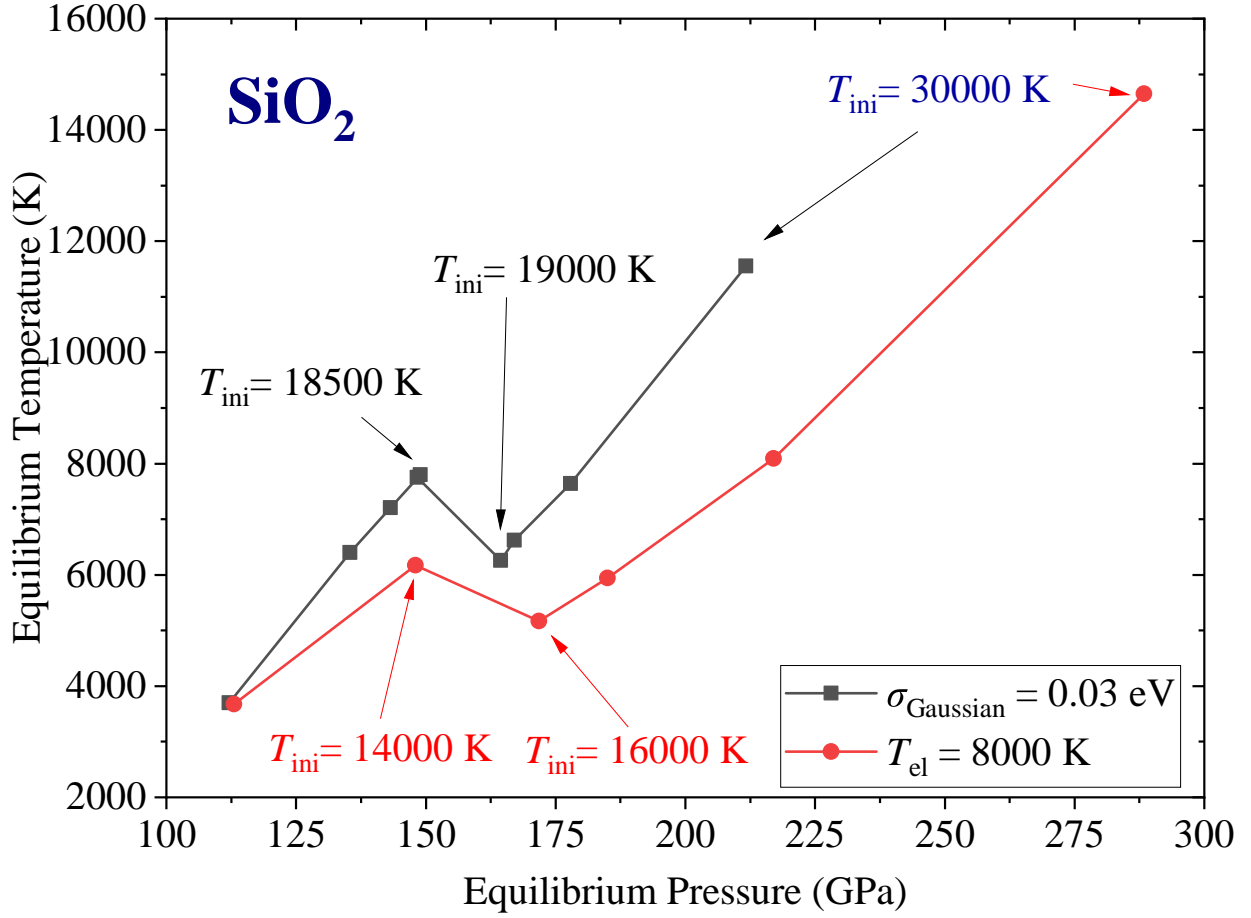


FIG. 2. Two fixed simulation time (20 ps) isochores with different electronic temperatures: (black curve $\sigma_{\text{Gaussian}} = 0.03$ eV) and red curve ($T_{\text{el}} = 8000 \approx T_{\text{m}}$). The initial temperatures span 8000 K to 30000 K with the ions initially placed at their ideal lattice positions.

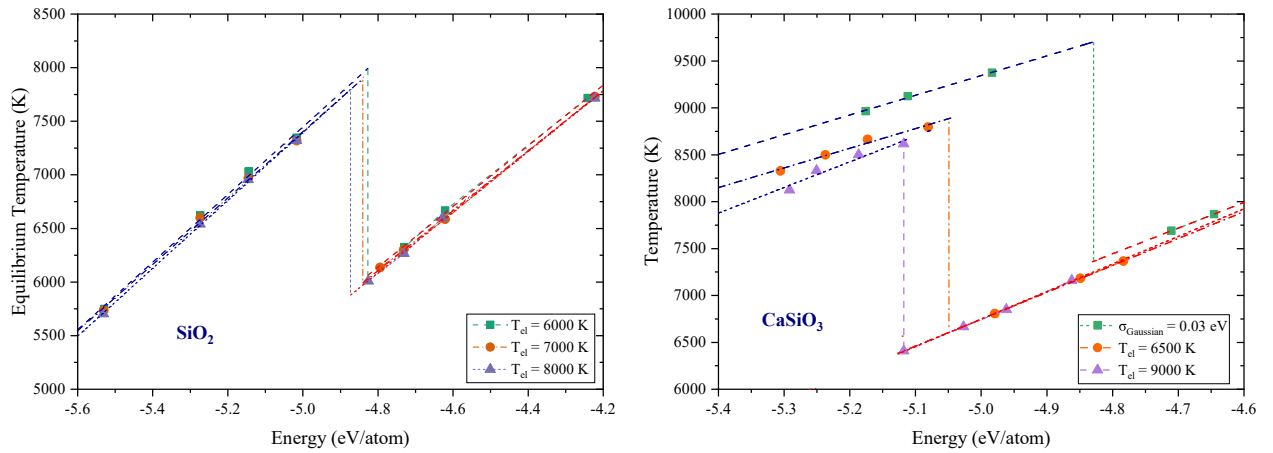


FIG. 3. Temperature vs. the total energy along solid (blue) and liquid (red) branches in MD-NVE runs for SiO_2 (left) and CaSiO_3 (right). For SiO_2 , $T_{\text{el}} = 6000$ K, 7000 K and 8000 K whereas for CaSiO_3 , T_{el} are 6500 K and 9000 K. In addition, we plot the result for CaSiO_3 with a Gaussian smearing scheme with $\sigma_{\text{Gaussian}} = 0.03$ eV. The resulting estimated homogeneous melting temperatures are reported in Table I.

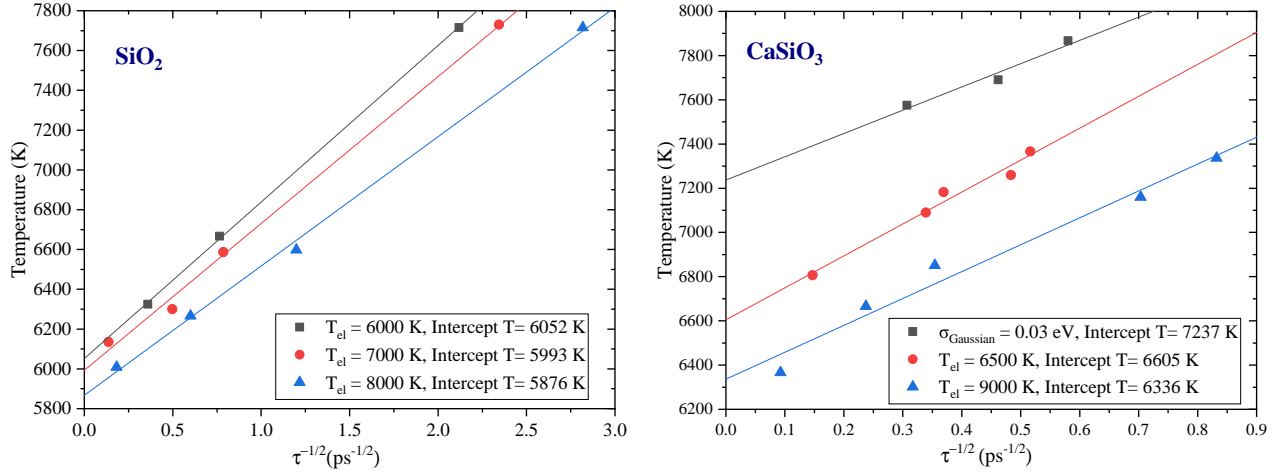


FIG. 4. Waiting time melting temperature analysis calculated using Eq. 3 for different choices of electronic temperatures. For SiO_2 , $T_{\text{el}} = 6000$ K, 7000 K and 8000 K whereas for CaSiO_3 T_{el} are 6500 K and 9000 K. In addition, we plot the waiting time for CaSiO_3 with a Gaussian smearing scheme with $\sigma_{\text{Gaussian}} = 0.03$ eV. The resulting estimated equilibrium melting temperatures are reported in Table I.

at the same thermodynamic conditions. Using the same exchange-correlation functional to DFT as in Ref. [17], we were unable to reproduce their melting point unless we set $T_{\text{el}} = T_{\text{ini}}$. Ref. [17], however, do not report values of T_{el} so no firm conclusions can be drawn.

D. SiO_2 melting

So far, there are not many experimental studies of SiO_2 that report melting temperatures to very high pressure. A recent high-pressure experimental study [47], fitted to an (equilibrium) melting curve to about 500 GPa ($T_m(P) = 1968.5 + 307.8 \times P^{0.485}$) is in quite good agreement with that from a Z method simulation [34] (i.e. $T_m(P) = 1968.5 + 478.7 \times P^{0.426}$). By contrast, a recent Diamond Anvil Cell (DAC) experiment [48, 49], suggests a markedly higher melting curve compared to those mentioned above and the Clapeyron slope is much steeper in the pressure region 120 - 150 GPa compared to that reported by Millot *et al* [47]. Molecular dynamics simulations [45, 46] using two-phase co-existing methods reported similar melting temperatures compared to the DAC study [48, 49], but without the rapid change in the Clapeyron slope claimed by the DAC experiment around 120 GPa. The melting temperatures for SiO_2 at a density of 5.305 g/cm³ are overall in good agreement with previous computational predictions at a similar pressure [45, 46]. The calculated melting temperature reported in Table I using $T_{\text{el}} = 8000$ K, for example, is 5776 K which is only slightly lower compared to those of Refs. [45] and [46] which are 5990 K and 5986 K respectively. Of note is that the good agreement with that reported by Usui and Tschuchia [46] may be fortuitous because a very small two-phase simulation box contain-

ing only 96 atoms was used in Ref. [46]. Such a small box has a boundary that is of similar size as the solid and liquid portions, and many runs are needed at a given (E, V) to precisely determine the melting points [50]. Our result also suggests that the predicted equilibrium melting curve from shock experiment [47] may be too low since it is assumed that stishovite is able to crystallize at the time-scale of the experiment and therefore drawn at the bottom of the liquid branch of the Hugoniot. If, however, stishovite is unable to crystallize at the time-scale of the shock-experiment (i.e. within a few nanoseconds) the melting-temperature may be underestimated as suggested by [51]. This interpretation is consistent with our calculated melting point.

As discussed above, the calculated melting temperature using $T_{\text{el}} = 8000$ K is slightly less than 200 K lower than that calculated using $T_{\text{el}} \approx T_h \approx 6000$ K. This difference in the calculated melting temperature is of similar size compared to that found for CaSiO_3 at similar conditions and confirms that the Z method may be hampered by some artificial feature for the accurate calculations of melting temperature with the Mermin free energy + ionic kinetic energy being conserved along the Born-Oppenheimer MD-NVE trajectory with T_{el} kept fixed.

E. Sensitivity to changes in electronic entropy on the waiting time analysis

The waiting time for the solid to melt is correctly described if we chose $T_{\text{el}} \approx \langle T \rangle_{\text{sol}}$ after equilibration (i.e. if, for example, $T_{\text{el}} = T_h$ when $E = E_h$). However, since the melting temperature is in general underestimated with $T_{\text{el}} = T_h$, interpolation to infinite waiting time using Eq. 3 gives a too low equilibrium melting temperature when τ is extrapolated to infinite waiting

System	Method	T_{el} (K)	P (GPa)	T_h (K)	T_m (K)	Ref.
CaSiO ₃	Z-Method	9000	103.7±2.6	8873	6315	This work
	Z-Method	6500	103.0±2.5	8652	6605	This work
	Z-Method	~0	105.2±3.0	9605	7237	This work
	Z-Method	adjust ^a	102.6±2.7	8506	6517	This work
	Z-Method	adjust ^b	105±3.3	8806	6493	Hernandez 2022 [22]
	Z-Method	not reported	103.0±0.2	7120	5200	Braithwaite 2019 [17]
	large-size co-existence		≈103		6582	Hernandez 2022 [22]
	Thermodynamic Integration		≈103		6433	Hernandez 2022 [22]
SiO ₂	2-Phase thermodynamics		≈103		5420	Hernandez 2022 [22]
	Coexist		153.8		5990	Benlonoshko 1995 [45]
	Coexist		157.6		5986	Usui 2010 [46]
	Shock Experiment		157.0		5543	Millot 2015 [47]
	Z-Method	not reported	132.331		5852	González-Cataldo 2016 [34]
	DAC Experiment		117		≈6200	Andrault et al. 2022 [48]
	Z-Method	6000	164±4.3	8058	6052	This Work
	Z-Method	7000	164±4.3	7899	5993	This Work
	Z-Method	8000	166±4.3	7789	5876	This Work
	Z-Method	Mixed	166		6134	This Work

TABLE I. Calculated melting temperature for CaSiO₃ and SiO₂ using the Z method together with previous values reported in the literature at similar pressure (i.e. about 103 GPa for CaSiO₃ and 160 GPa for SiO₂). In the simulation where $T_{el} \sim 0$ we used Gaussian smearing, $\sigma_{\text{gauss}} = 0.03$ eV, for the partial occupancies of the one-electron orbitals. In the simulation from Ref. [22] where T_{el} is labelled as "adjust^b", the Fermi-Dirac smearing was updated about every 1 ps along the MD trajectory to match the average temperature in the previous ~ 1 ps, as discussed in Ref. [22]. In "adjust^a" we update the electronic entropy only once along the MD trajectory.

time. However, if we use a lower T_{el} (i.e. if we chose $T_{el} = \langle T \rangle_{\text{liq}}$) the waiting time for the system to melt will be too slow. This implies that $\tau^{-1/2}$ should be shifted to lower temperatures indicating that the melting temperature calculated from the intersection $\tau^{-1/2} = 0$ will be overestimated. The estimated melting temperature with $T_{el} \approx T_m$ and $T_{el} \approx T_h$, therefore, provide upper and lower bounds respectively to the "true" equilibrium melting temperature.

To better quantify these errors we can follow a similar strategy as in Ref.[22] by adjusting the electronic entropy along the Born-Oppenheimer MD trajectory to match the new average ionic temperature after transition to the liquid state. We relaunched MD runs where $T_{el} \approx T_h$ with $E \approx E_h$ after melting, by decreasing the electronic temperature to match the average liquid temperature after some propagation in the liquid state. In Fig. 5 (top panel) we show one such example for CaSiO₃ where $\langle T \rangle$ (after melting) is very close to the estimated melting temperature from the waiting time analysis; in this run $\langle T \rangle_{\text{liq}} = 6408$ K with $T_{el} = 9000$ K which is close to T_m . After 25 ps in the liquid state, we restarted this run (blue line) with $T_{el} = 6500$ K. The average liquid temperature increased by about 100 K (to 6517 K). At the same time, the total energy increased markedly by about 1%. The $\langle T \rangle_{\text{liq}}$ from this MD run (blue line) is higher and lower respectively than the melting temperature reported in Table I for $T_{el} = 9500$ K and $T_{el} = 6500$ K respectively.

Fig. 5 for SiO₂ also demonstrates that changes in electronic entropy can have a huge impact on the ionic dynamics. Here we relaunch the simulation by changing

the electronic temperatures from 7000 K (green line) to $T_{el} = 6000$ K or $T_{el} = 8000$ K. The MD run with $T_{el} = 6000$ K froze after about 15 ps of propagation in the liquid state whereas the simulation with $T_{el} = 8000$ K remained stable in the liquid phase until the run was terminated after more than 35 ps.

F. Solid-liquid oscillations

Although solid-liquid transitions may be triggered by small changes in electronic entropy, refreezing can also occur spontaneously in *NVE* runs when the temperature fluctuations are large. That is, when there is an overlap between liquid and solid temperature distributions as discussed in Ref. [20]. Fig. 6 illustrates solid-liquid oscillations for SiO₂. Here the temperature drops after about 20 ps as the system melts, followed by a 30 ps evolution in the liquid state before the system rapidly recrystallizes. After 10 ps in the solid state, it melts again and remains stable in the melt for more than 20 ps before the run is terminated. Since, however, the temperature fluctuations scale as $1/\sqrt{N}$ (where N is the number of atoms in the simulation box), the overlap between the solid and liquid temperatures decreases with increasing box size and hence the frequency of the solid-liquid alternation decreases. Oscillation on a time scale of nanoseconds or less is therefore usually only seen in MD runs carried out in small simulation boxes (~ 100 atoms).

An interesting implication of such solid-liquid oscillation is that it is possible to estimate the melting temperature by targeting the total energy in which the system

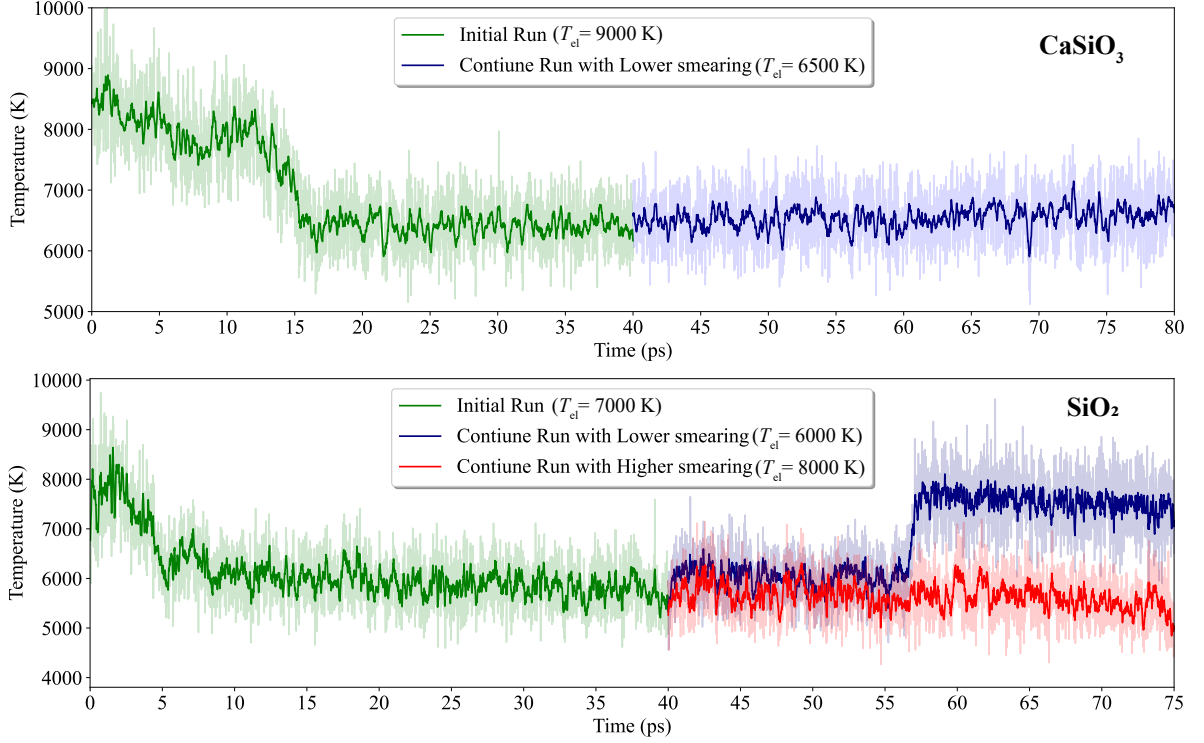


FIG. 5. Blue and red lines are continuation runs after about 40 ps of simulations (green lines) where the simulations restarted with the same atomic positions and forces as the last step of the initial (green) run but with different electronic temperatures. For CaSiO_3 , the MD run was launched (green line) with $T_{\text{el}} = 9000$ K and then continued with $T_{\text{el}} = 6500$ K (blue line). For SiO_2 we started with $T_{\text{el}} = 7000$ K (green line) and then continued with $T_{\text{el}} = 6000$ K (blue line) and 8000 K (red line).

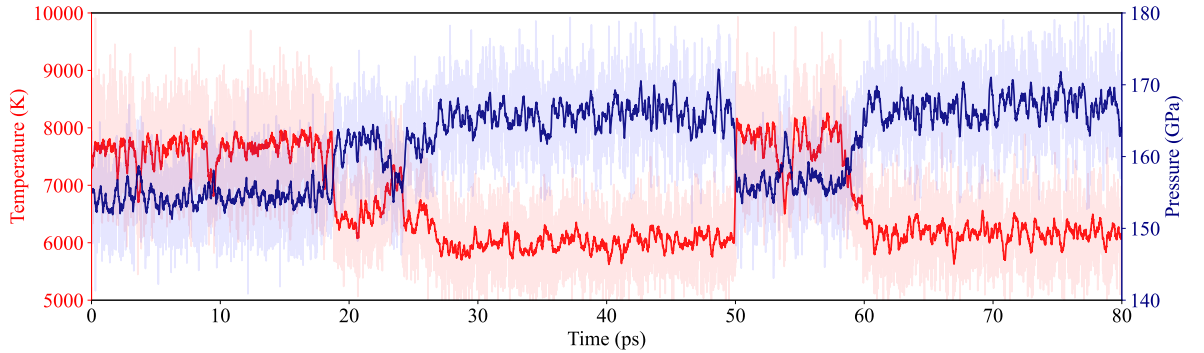


FIG. 6. Temperature and pressure evolution in an SiO_2 MD run where $T_{\text{ini}} = 17000$ K and $T_{\text{el}} = 8000$ K. Transition between liquid and solids take place at 25 ps, 50 ps and 60 ps. Note the overlapping fluctuations in temperature/pressure along solid and liquid states.

spends an equal amount of time in the solid and liquid phases. In this case, the entropy of the two phases are equal and hence the melting temperature can be extracted directly from the MD run [20]. However, in our case of SiO_2 melting at ~ 160 GPa, extremely long runs - probably on the size of tens of nanoseconds - would be needed to collect sufficient statistics. In addition, analy-

sis of all trajectories shows that liquid-solid transition is rare in NVE MD runs in SiO_2 , and for CaSiO_3 we did not observe any re-crystallization events even though the size of the simulation box size is modest (135 atoms).

G. Homogeneous sub-lattice melting and defect formation

Inspection of ionic trajectories in the two systems studied here allows a details insight into homogeneous melt-nucleation and shows that homogeneous melting takes place via a two-step mechanism. First, the anion-sublattice melt which is accompanied by a small drop in temperature. Next, small cation defects form which trigger the nucleation of small liquid clusters and full melting accompanied by a large drop in temperature. Evidence for the initial homogeneous sub-lattice melting of the oxygens is illustrated in Fig. 7 for SiO_2 . The MSDs of the individual sub-lattices shows that the oxygen lattice melts several ps before the entire system melts. In the case of SiO_2 , homogeneous sublattice-melting is accompanied by a small, but distinct, drop in temperature as seen in the figure, whereas for CaSiO_3 the temperature drop is not easily visible in the average temperature. This temperature drop suggests that the ideal homogeneous melting temperature estimated from a *linear extrapolation* along the solid branch (using Eq. 2 and shown in Fig 3) is likely to be overestimated. Molten sublattices may therefore explain the change in slope along the solid branch near the limit of supercritical melting seen in many systems [17, 19].

In Fig. 8 we show in more detail a typical homogeneous melting mechanism of SiO_2 and CaSiO_3 captured in the MD runs. In the case of CaSiO_3 , we frequently see that pairs of different cations exchange position or a cation is excited into an interstitial site. Small, short-ranged and short-lived (~ 0.5 ps), liquid-like clusters often form soon thereafter before the entire system melts. For SiO_2 the liquid-like cluster is typically formed from a cooperative excitation where a silicon (marked as "1" in Fig. 8) is moving in the direction of another silicon (i.e. silicon "2" in Fig. 8) where it "kicks" silicon "2" out of its cavity. Although our simulation box is too small to capture the tail of the growth stage, the small glass-like nuclei appears to be fully embedded in the simulation box.

Since inspection of ionic trajectories in the two systems studied here indicates that the formation of small liquid clusters above T_h , in general, involve only a very few atoms, small or modest sized simulation boxes are often sufficient to capture the homogeneous melting processes. This highlights the potential power of the Z method in accurately calculating melting points at low computational cost.

V. CONCLUSIONS

In this work, we used the Z method together with *ab initio* Born-Oppenheimer molecular dynamics to calculate the melting temperature for SiO_2 and CaSiO_3 at outer core and lower mantle conditions respectively using the Z methods with simulation boxes containing ~ 100 atoms only. The calculated melting temperature

for CaSiO_3 is in excellent agreement with previously reported two-phase co-existence calculations and thermodynamic integration and is substantially higher than a previous *ab initio* study using the Z method [17]. A possible explanation for this discrepancy has been discussed. The calculated melting temperature for SiO_2 is also in overall good agreement with previous computational work carried out at similar pressure and temperature suggesting that the previous estimated equilibrium melting temperature may be too high [47]

One of the great advantages of using the Z method compared to other popular methods to melting such as two-phase simulations and thermodynamic integration is that the homogeneous melting temperature and hence the equilibrium melting temperature can be accurately calculated using small- or modest-sized simulation boxes. This is because melting near T_h is in general triggered by small liquid nuclei that can be embedded in a small simulation box. Indeed, inspection of the MD trajectories show that small liquid nuclei form after homogeneous melting of the oxygen sublattice which initiates the "irreversible" and rapid homogeneous melting of the entire system. In contrast, direct simulation of equilibrium melting often involves extended surfaces or grain boundaries which require large simulation boxes to accommodate both phases including their interface.

The observation of homogeneous melting of entire sublattices before melt nuclei is formed has to our knowledge not previously been observed computationally or experimentally and challenge the conventional atomistic model of homogeneous melting processes.

Additional potential strengths of the Z methods have been highlighted. Since the melting temperature is obtained from the relationship between T_h and T_m using Eq.1, the Z method avoids the calculation of free energies which can be extremely tedious and expensive. Moreover, the Z method can easily be implemented and interfaced with popular *ab initio* simulation software such as VASP and is embarrassingly parallelizable.

In spite of many appealing advantages compared to other methods to melting, the Z method appears to be hampered by some artificial features which needs to be much better addressed. One of these, investigated here, is the choice of electronic entropy in Born-Oppenheimer MD simulation carried out in the microcanonical ensemble when $K + \Omega$ is a conserved and hence T_{el} is kept fixed along the Hellmann-Feynman trajectory. Since melting is accompanied by a large drop in temperature we need to quantify the errors introduced due to the choice of electronic temperature/entropy. We, therefore, compare the melting temperature calculated using $T_{el} \approx T_h$ and $T_{el} \approx T_m$ since these represent reasonable upper and lower bounds to the "true" melting temperature. For SiO_2 and CaSiO_3 at high pressure and temperature, the difference in the calculated T_m with $T_{el} \approx T_h$ and $T_{el} \approx T_m$ is about 200-300 K. Although these discrepancies are only a few percent of the melting temperature, they are not negligible for the accurate calculation

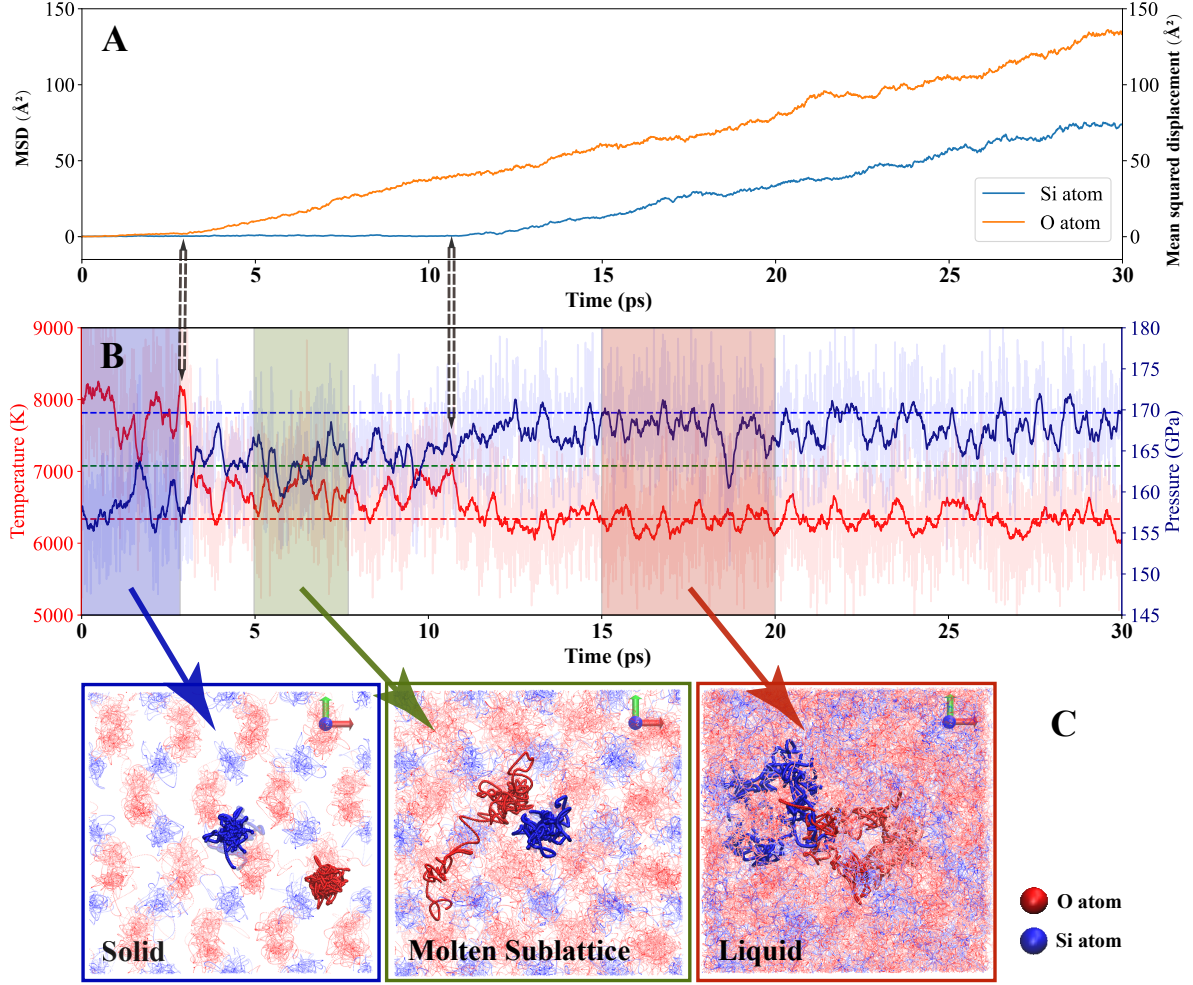


FIG. 7. Panel A shows a MSD plot illustrating sublattice melting in SiO_2 where $T_{\text{ini}} = 18000\text{K}$ and $T_{\text{el}} = 7000\text{K}$. B shows the temperature and pressure profile along the trajectory whereas the trajectory over the coloured area (blue, green and red) is shown in C. Here a single silicon and oxygen atom are highlighted to better visualize the trajectories at different steps during melting.

of melting temperature and are important to take into account for a critical assessment of the Z method implemented together with Born-Oppenheimer MD in the NVE ensemble with a constant electronic temperature.

ACKNOWLEDGMENTS

We thank Prof. Dario Alfè for the thoughtful discussion. The Centre for Earth Evolution and Dynamics is funded by the Research Council of Norway through its Centre of Excellence program (Grant 223272). We acknowledge financial support from the Research Council of Norway through its Centres of Excellence scheme, project number 332523 (PHAB). Computational resources were provided by the Norwegian infrastructure for high-performance computing (NOTUR, Sigma-2, Grants NN9329K and NN2916K).

[1] A. B. Belonoshko, N. V. Skorodumova, A. Rosengren, and B. Johansson, Melting and critical superheating,

Physical Review B **73**, 012201 (2006).

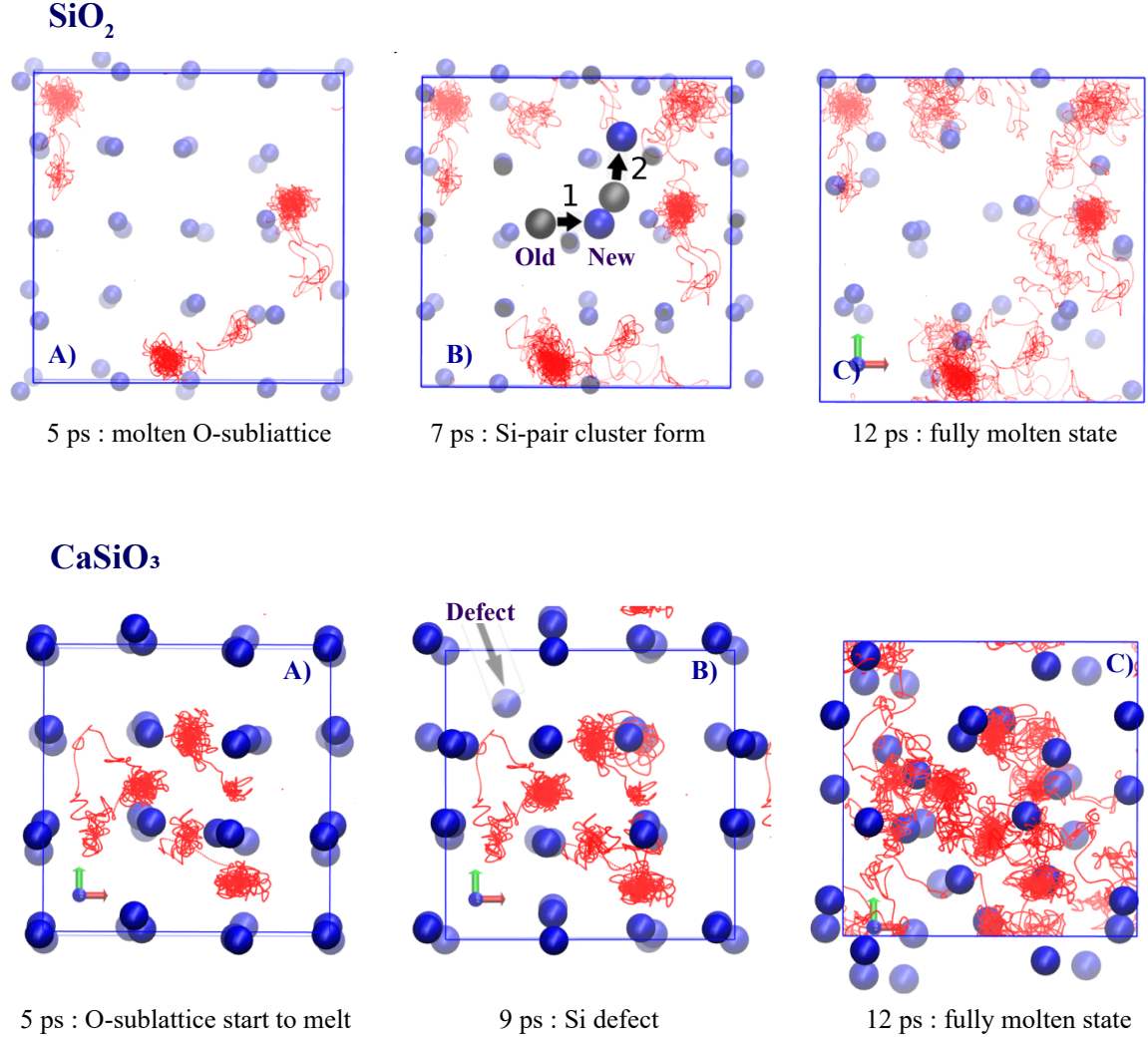


FIG. 8. Examples of homogeneous melting mechanism in SiO₂ and CaSiO₃. Only 3 oxygens are shown and the calcium-atoms in CaSiO₃ are omitted for clarity. SiO₂: A) shows that the oxygen sub-lattice starts to melt without diffusion of any silicons; B) shows that melting nucleation is triggered by a cooperative pair of silicons that initial melting until; C) the entire system has melted. CaSiO₃: A) shows that the oxygen sub-lattice starts to melt without any diffusion of the cations; B) shows that interstitial defects Si-defect form which trigger melt nucleation and a few ps later; C) the entire system has melted.

- [2] V. Olguín-Arias, S. Davis, and G. Gutierrez, Extended correlations in the critical superheated solid, *The Journal of Chemical Physics* **151**, 10.1063/1.5111527 (2019).
- [3] C. J. Rossouw and S. E. Donnelly, Superheating of small solid-argon bubbles in aluminum, *Phys. Rev. Lett.* **55**, 2960 (1985).
- [4] J. B. Boyce and M. Stutzmann, Orientational ordering and melting of molecular h₂ in an α -si matrix: Nmr studies, *Physical Review Letters* **54**, 562 (1985).
- [5] R. W. Cahn, Materials science: Melting and the surface, *Nature* **323**, 668 (1986).
- [6] J. H. Evans and D. J. Mazey, Solid bubble formation in titanium injected with krypton ions, *Journal of Nuclear Materials* **138**, 176 (1986).
- [7] A. R. Finney and P. M. Rodger, Applying the z method to estimate temperatures of melting in structure ii clathrate hydrates, *Physical Chemistry Chemical Physics* **13**, 19979 (2011).
- [8] B. K. Benazzouz, A. Zaoui, and A. B. Belonoshko, Determination of the melting temperature of kaolinite by means of the z-method, *American Mineralogist* **98**, 1881 (2013).
- [9] F. Saiz, An ab initio study on liquid silicon carbide, *Journal of Physics and Chemistry of Solids* **137**, 109204 (2020).
- [10] S. R. Baty, L. Burakovsky, and D. Errandonea, Ab initio phase diagram of silver, *Journal of Physics: Condensed Matter* **33**, 485901 (2021).
- [11] J. Bouchet, F. Bottin, G. Jomard, and G. Zerah, Melting curve of aluminum up to 300 gpa obtained through ab

- initio molecular dynamics simulations, *Physical Review B* **80**, 094102 (2009).
- [12] A. B. Belonoshko and A. Rosengren, High-pressure melting curve of platinum from ab initio z method, *Physical Review B* **85**, 174104 (2012).
 - [13] H. Y. Geng, R. Hoffmann, and Q. Wu, Lattice stability and high-pressure melting mechanism of dense hydrogen up to 1.5 tpa, *Physical Review B* **92**, 104103 (2015).
 - [14] L. Burakovsky, N. Burakovsky, and D. L. Preston, Ab initio melting curve of osmium, *Physical Review B* **92**, 174105 (2015).
 - [15] Y. Zhang, Y. Tan, H. Y. Geng, N. P. Salke, Z. Gao, J. Li, T. Sekine, Q. Wang, E. Greenberg, V. B. Prakapenka, and J.-F. Lin, Melting curve of vanadium up to 256 gpa: Consistency between experiments and theory, *Physical Review B* **102**, 214104 (2020).
 - [16] D. V. Minakov, M. A. Paramonov, G. S. Demyanov, V. B. Fokin, and P. R. Levashov, Ab initio calculation of hafnium and zirconium melting curves via the lindemann criterion, *Physical Review B* **106**, 214105 (2022).
 - [17] J. Braithwaite and L. Stixrude, Melting of casio₃ perovskite at high pressure, *Geophysical Research Letters* **46**, 2037 (2019).
 - [18] S. M. Stishov, I. N. Makarenko, V. A. Ivanov, and A. M. Nikolaenko, On the entropy of melting, *Physics Letters A* **45**, 18 (1973).
 - [19] S. Davis, S. , Loyola, and P. J., Bayesian statistical modeling of microcanonical melting times at the superheated regime, *Physica A* **515**, 546 (2019).
 - [20] D. Alfé, C. Cazorla, and M. J. Gillan, The kinetics of homogeneous melting beyond the limit of superheating, *The Journal of Chemical Physics* **135**, 024102 (2011).
 - [21] F. González-Cataldo, S. Davis, and G. Gutierrez, Z method calculations to determine the melting curve of silica at high pressures, *Journal of Physics: Conference Series* **720**, 012032 (2016).
 - [22] J.-A. Hernandez, C. E. Mohn, M. G. Guren, M. A. Baron, and R. G. Trønnes, Ab initio atomistic simulations of ca-perovskite melting, *Geophysical Research Letters* **49**, e2021GL097262 (2022).
 - [23] C. Di Paola and J. P. Brodholt, Modeling the melting of multicomponent systems: the case of mgsio₃ perovskite under lower mantle conditions, *Scientific Reports* **6**, 29830 (2016).
 - [24] B. Grabowski, L. Ismer, T. Hickel, and J. Neugebauer, Ab initio up to the melting point: Anharmonicity and vacancies in aluminum, *Physical Review B* **79**, 134106 (2009).
 - [25] A. I. Duff, T. Davey, D. Korbacher, A. Glensk, B. Grabowski, J. Neugebauer, and M. W. Finnis, Improved method of calculating ab initio high-temperature thermodynamic properties with application to zrc, *Physical Review B* **91**, 214311 (2015).
 - [26] S.-T. Lin, M. Blanco, and I. Goddard, William A., The two-phase model for calculating thermodynamic properties of liquids from molecular dynamics: Validation for the phase diagram of lennard-jones fluids, *The Journal of Chemical Physics* **119**, 11792 (2003).
 - [27] L.-F. Zhu, B. Grabowski, and J. Neugebauer, Efficient approach to compute melting properties fully from ab initio with application to cu, *Physical Review B* **96**, 224202 (2017).
 - [28] A. de Vita, The energetics of defects and impurities in metal and ionic materials from first principles, PhD Thesis, Keele University (1992).
 - [29] R. M. Wentzcovitch, J. L. Martins, and P. B. Allen, Energy versus free-energy conservation in first-principles molecular dynamics, *Physical Review B* **45**, 11372 (1992).
 - [30] M. Weinert and J. W. Davenport, Fractional occupations and density-functional energies and forces, *Physical Review B* **45**, 13709 (1992).
 - [31] A. Corgne, C. Liebske, B. J. Wood, D. C. Rubie, and D. J. Frost, Silicate perovskite-melt partitioning of trace elements and geochemical signature of a deep perovskitic reservoir, *Geochimica et Cosmochimica Acta* **69**, 485 (2005).
 - [32] S. Tateno, K. Hirose, S. Sakata, K. Yonemitsu, H. Ozawa, T. Hirata, N. Hirao, and Y. Ohishi, Melting phase relations and element partitioning in morb to lowermost mantle conditions, *Journal of Geophysical Research: Solid Earth* **123**, 5515 (2018).
 - [33] P. K. Das, C. E. Mohn, J. P. Brodholt, and R. G. Trønnes, High-pressure silica phase transitions: Implications for deep mantle dynamics and silica crystallization in the protocore, *American Mineralogist* **105**, 1014 (2020).
 - [34] F. González-Cataldo, S. Davis, and G. Gutierrez, Melting curve of sio₂ at multimegabar pressures: implications for gas giants and super-earths, *Scientific Reports* **6**, 26537 (2016).
 - [35] K. Hirose, Crystallization of silicon dioxide and compositional evolution of the earth's core, *Nature* **543**, 99 (2017).
 - [36] R. G. Trønnes, M. A. Baron, K. R. Eigenmann, M. G. Guren, B. H. Heyn, A. Løken, and C. E. Mohn, Core formation, mantle differentiation and core-mantle interaction within earth and the terrestrial planets, *Tectonophysics* **760**, 165 (2019).
 - [37] N. D. Mermin, Thermal properties of the inhomogeneous electron gas, *Physical Review* **137**, A1441 (1965).
 - [38] G. Kresse and J. Hafner, Ab initio molecular dynamics for liquid metals, *Physical Review B* **47**, 558 (1993).
 - [39] G. Kresse and J. Hafner, Ab initio molecular-dynamics simulation of the liquid-metal-amorphous-semiconductor transition in germanium, *Physical Review B* **49**, 14251 (1994).
 - [40] P. E. Blöchl, Projector augmented-wave method, *Physical Review B* **50**, 17953 (1994).
 - [41] G. Kresse and D. Joubert, From ultrasoft pseudopotentials to the projector augmented-wave method, *Physical Review B* **59**, 1758 (1999).
 - [42] J. P. Perdew, K. Burke, and M. Ernzerhof, Generalized gradient approximation made simple, *Physical Review Letters* **77**, 3865 (1996).
 - [43] R. Armiento and A. E. Mattsson, Functional designed to include surface effects in self-consistent density functional theory, *Phys. Rev. B* **72**, 085108 (2005).
 - [44] D. Alfé, Melting curve of mgo from first-principles simulations, *Phys. Rev. Lett.* **94**, 235701 (2005).
 - [45] A. B. Belonoshko and L. S. Dubrovinsky, Molecular dynamics of stishovite melting, *Geochimica et Cosmochimica Acta* **59**, 1883 (1995).
 - [46] Y. Usui and T. Tsuchiya, Ab initio two-phase molecular dynamics on the melting curve of sio₂, *Journal of Earth Science* **21**, 801 (2010).
 - [47] M. Millot, N. Dubrovinskaya, A. Černok, S. Blaha,

- L. Dubrovinsky, D. G. Braun, P. M. Celliers, G. W. Collins, J. H. Eggert, and R. Jeanloz, Shock compression of stishovite and melting of silica at planetary interior conditions, *Science* **347**, 418 (2015).
- [48] D. Andrault, L. Pison, G. Morard, G. Garbarino, M. Mezouar, M. A. Bouhifd, and T. Kawamoto, Comment on: Melting behavior of SiO_2 up to 120 gpa (andrault et al. 2020), *Physics and Chemistry of Minerals* **49**, 3 (2022).
- [49] D. Andrault, G. Morard, G. Garbarino, M. Mezouar, M. A. Bouhifd, and T. Kawamoto, Melting behavior of SiO_2 up to 120 gpa, *Physics and Chemistry of Minerals* **47**, 10 (2020).
- [50] Q.-J. Hong and A. van de Walle, A user guide for sluschi: Solid and liquid in ultra small coexistence with hovering interfaces, *Calphad* **52**, 88 (2016).
- [51] Y. Shen, S. B. Jester, T. Qi, and E. J. Reed, Nanosecond homogeneous nucleation and crystal growth in shock-compressed SiO_2 , *Nature Materials* **15**, 60 (2016).
- [52] C. E. Mohn, S. Stølen, and S. Hull, Diffusion within α -CuI studied using ab initio molecular dynamics simulations, *Journal of Physics: Condensed Matter* **21**, 335403 (2009).
- [53] C. E. Mohn, S. Stølen, S. T. Norberg, and S. Hull, Ab initio molecular dynamics simulations of oxide-ion disorder in the δ - Bi_2O_3 , *Phys. Rev. B* **80**, 024205 (2009).
- [54] D. Alfé, M. J. Gillan, and G. D. Price, Complementary approaches to the ab initio calculation of melting properties, *The Journal of Chemical Physics* **116**, 6170 (2002).
- [55] A. Wilson and L. Stixrude, Entropy, dynamics, and freezing of CaSiO_3 liquid, *Geochimica et Cosmochimica Acta* **302**, 1 (2021).
- [56] G. Zhang, X. Fan, Q. Zhang, Q. Li, Y. Wu, and M. Li, Partial disordering and homogeneous melting in multi-component systems, *Acta Materialia* **239**, 118281 (2022).
- [57] A. B. Belonoshko, L. Burakovsky, S. P. Chen, B. Johansson, A. S. Mikhaylushkin, D. L. Preston, S. I. Simak, and D. C. Swift, Molybdenum at high pressure and temperature: Melting from another solid phase, *Physical Review Letters* **100**, 135701 (2008).
- [58] A. D. Rabuck and G. E. Scuseria, Improving self-consistent field convergence by varying occupation numbers, *The Journal of Chemical Physics* **110**, 695 (1999).
- [59] G. Kresse and J. Furthmüller, Efficient iterative schemes for ab initio total-energy calculations using a plane-wave basis set, *Physical Review B* **54**, 11169 (1996).
- [60] G. Kresse and J. Furthmüller, Efficiency of ab-initio total energy calculations for metals and semiconductors using a plane-wave basis set, *Computational Materials Science* **6**, 15 (1996).
- [61] G. Levi, A. V. Ivanov, and H. Jónsson, Variational density functional calculations of excited states via direct optimization, *Journal of Chemical Theory and Computation* **16**, 6968 (2020).
- [62] M. R. Pederson and K. A. Jackson, Pseudoenergies for simulations on metallic systems, *Physical Review B* **43**, 7312 (1991).

Free energy conservation in *ab initio* molecular dynamics simulations and homogeneous melt nucleation

Supplementary Information

Ming Geng¹ and Chris E. Mohn^{1,2,*}

¹*The Centre for Earth Evolution and Dynamics (CEED) and Centre for Planetary Habitability (PHAB), University of Oslo, N-0315 Oslo, Norway and*

²*Department of Chemistry and Center for Materials Science and Nanotechnology, University of Oslo, Oslo 0371, Norway*

A. Distribution of waiting times

The use of the waiting time analysis via Eq. 3 provides a powerful implementation of the Z method, but a substantial amount of statistics is still needed for the precise calculation of T_m . The stochastic nature of melting and long tails in the waiting time distribution remains a challenge to the Z method Refs. [19, 20]. As can be seen in the inset in Fig. S1 (where the liquid temperature is about 250 K higher than T_m with $T_{\text{ini}} = 20000$ K, $T_{\text{el}} = 6500$ K), some calculations melted fairly quickly (< 10 ps) whereas other remained stable for more the 200 ps. Although we do not have sufficient statistics to capture the functional form of the distribution of τ , analysis carried out by Davis *et al* [19] showed - using a classical Lennard-Jones potential to model melting of Ar - that the distribution of τ appears to be gamma-like rather than exponential.

Although exponential decays describe many dynamical atomistic processes such as hopping events in solids [52, 53], the time taken from random fluctuations that trigger melting to when melting is observed will always take a certain time [19]. This suggests that τ deviates from an exponential decay at short times [19]. In Fig. S1 and S2, we plot the distribution of the waiting times and possible

(fitted) distributions for CaSiO_3 and SiO_2 respectively. The plots confirm that the melting time is sensitive to initial temperature and electronic entropy as discussed above. The distributions of τ with T_{el} close to T_m are wide and with standard deviations which are on the size of the average waiting time. For CaSiO_3 where $T_{\text{ini}} = 20000$ K and $T_{\text{el}} = 6500$ K (Fig S1), for example, the mean waiting time is ~ 50 ps with standard deviations of about 60 ps.

If we assume that the waiting time can be precisely determined by Eq. 3 a fruitful strategy to minimize the computational cost in a waiting time analysis would be to choose the total energies/initial temperatures such that $\tau < 10$ ps and $\tau > \tau_{\text{melting}}$ ps. The upper bound ensures that we minimize lengthy MD runs, whereas the lower bound ensures that the waiting time is markedly longer than the time it takes from nucleation precursors triggering the formation of liquid nuclei until the entire system has melted (τ_{melting}) which is typical ~ 1 ps. (see Fig.1 in the main text). The lower bounds are (useful) because it is not always straightforward to estimate the value of τ_{melting} . This is partly because thermal fluctuations make it difficult to precisely identify the value of τ_{melt} in a given run and partly because different mechanisms may trigger melting and these may have very different waiting times as discussed in the main text.

* chrism@kjemi.uio.no

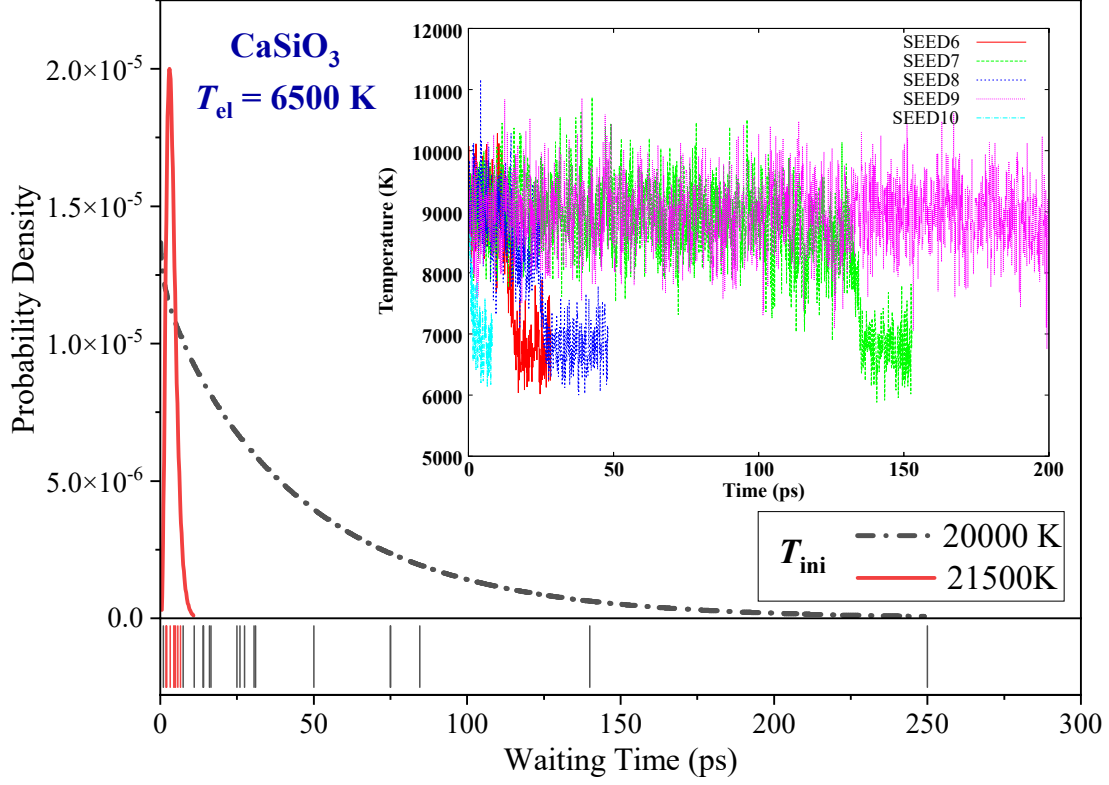


FIG. S1. Distribution of waiting times for melting and example of NVE MD runs of CaSiO_3 with $T_{\text{ini}} = 20000 \text{ K}$ and $T_{\text{el}} = 6500 \text{ K}$. A gamma-type function is fitted to the distribution probability density. The inset figure shows five different seeds of the temperature evolution in an NVE MD runs with $E > E_h$ for CaSiO_3 . In all runs the atoms were located at their equilibrium positions and the velocities were drawn from a Maxwell-Boltzmann distribution.

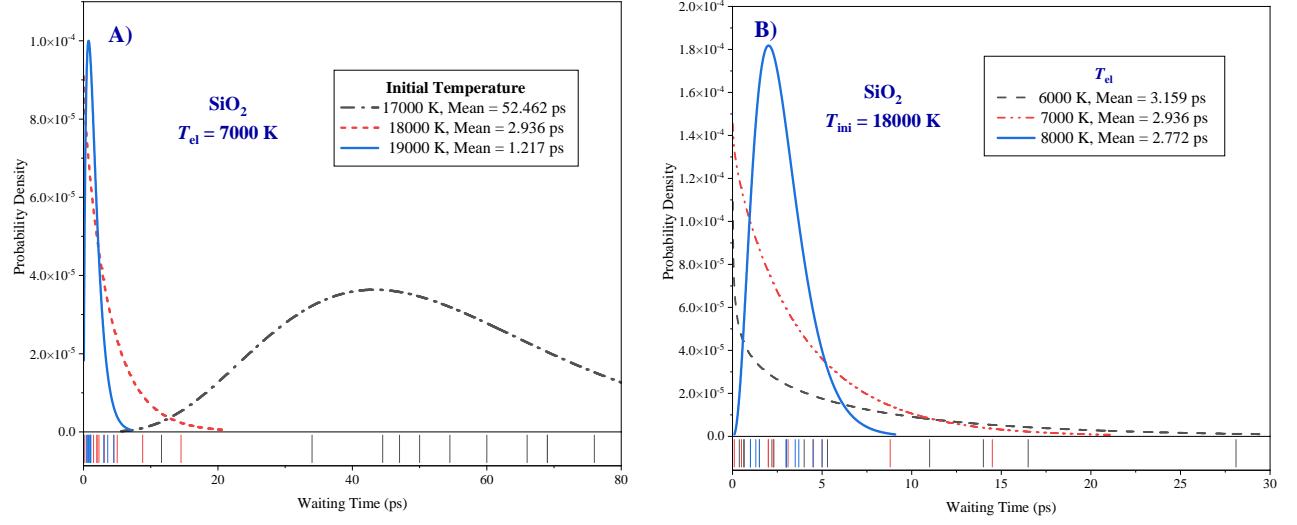


FIG. S2. Distribution of waiting times for melting of SiO_2 . A gamma-type function is fitted to the distribution probability density. The left one collect results from runs with the same electronic temperature but different initial temperature and the right one are with the same initial temperature but different electronic temperatures. In all runs the atoms were located at their equilibrium positions and the velocities were drawn from a Maxwell-Boltzmann distribution.